Polycrystalline Vanadium Oxide Nanorods: Growth, Structure and Improved Electrochemical Response as a Li-Ion Battery Cathode Material

D. McNulty,[a,b] D. N. Buckley,[a,b,c,*] and C. O'Dwyer[c,d,e,,z]**

[a]*Department of Physics and Energy, University of Limerick, Limerick, Ireland*
[b]*Charles Parsons Initiative on Energy and Sustainable Environment, University of Limerick, Limerick, Ireland*
[c]*Materials & Surface Science Institute, University of Limerick, Limerick, Ireland*
[d]*Department of Chemistry, University College Cork, Cork, Ireland*
[e]*Micro & Nanoelectronics Centre, Tyndall National Institute, Lee Maltings, Cork, Ireland*

Thermally removing amine molecules that serve as chemical templates for vanadium oxide nanotubes is demonstrated to significantly improve the performance when tested as a cathode material in Li-ion battery cells. Capacity fading issues associated with blocked intercalation sites on the (010) faces of layered vanadium oxide that form the nanotubes are prevented. Thermal treatment of the nanotubes up to 600°C is shown to cause a specific conversion from nanotubes to polycrystalline nanorods and removal of the organic template. The conversion process was monitored by thermogravimetric analysis, X-ray diffraction, transmission electron microscopy and infra-red spectroscopy. In a potential window of 4.0–1.2 V drawing 30 μA (C/30), the nanorods show improved specific capacities of ∼280 mAh g^{-1} with a modest 6% capacity fade compared to ∼8 mAh g^{-1} with 62% capacity fade for the VONTs. The improvements in specific capacity and cycling performance are due to the successful removal of amine molecules and conversion to nanorods containing nanoscale crystals. The cathode material also demonstrated enhanced energy densities (∼700 W h kg^{-1}) compared to composites of the same overall weight, without conductive carbon additives or polymeric binders.

Manuscript submitted April 17, 2014; revised manuscript received May 27, 2014. Published June 13, 2014. This was in part Paper 717 presented at the Honolulu, Hawaii, Meeting of the Society, October 7–12, 2012.

In recent years there has been a significant increase in the desire and need to improve the performance and cycle life of commercial rechargeable lithium ion batteries.[1–6] The advent of smart phones and tablet devices has highlighted the limitations of current generation lithium ion batteries. Rechargeable lithium ion batteries still hold great promise for use in powering electric and hybrid electric vehicles and continue to be crucial in medical and handheld portable devices.[7] However it is vital that factors such as power and energy density, coulometric efficiency and rate performance are improved upon in order to meet demands for improved performance in advanced Li-ion batteries (∼400 Wh/kg).[1,4,7–9] It is no surprise that nanostructured materials are attracting significant attention because of their novel properties and their potential applications in a wide range of devices such as biological and gas sensors,[10–18] field effect transistors[19,20] and as electrode materials for next generation high energy density batteries.[21–23] Nanostructured cathode electrodes offer improved energy storage capacity and charge–discharge kinetics, as well as better cyclic stabilities.[24] This is, in part, due to the increased surface area in direct contact with the electrolyte, and better electronic and ionic conductivity, and shorter distances for cation diffusion as compared with bulk materials.[25] Nanostructured electrodes are also able to better accommodate volume changes associated with cyclic intercalation and deintercalation of lithium ions into and from the host lattice. This reduces pulverization issues associated with bulk materials and consequently improves cycle life.[2]

Vanadium oxides and their derivative compounds have attracted special attention because of their outstanding physical and chemical properties and potential applications in various areas, such as catalysts,[25–30] sensors[31–38] and electrodes.[39–47] The magnetic and optical properties of vanadium oxide nanotubes (VONTs) have also been thoroughly investigated.[36,48–52] In particular one-dimensional nanostructured vanadium oxide materials such as nanofibers[53,54] and nanobelts[31,55] as well as nano-urchin,[43,56] nanorods[57,58] and nanotubes[59–61] are being extensively studied as cathode materials due to their unique geometry,[26] low cost, facile preparation and large specific capacity.[62] Nanostructures such as vanadium oxide nanotubes (VONTs) and nanorods are particularly attractive in principle as they provide several access regions and facile intercalation sites for cations and in defective form as redox pseudocapacitive charge storage to boost energy density.[63–66] This large surface area-to-volume ratio ideally should facilitate a greater area of vanadium oxide in direct contact with the electrolyte as compared with bulk vanadium oxide.[67] When coupled with the nano-scale dimensions of the VONTs which facilitate shorter diffusion lengths for Li ions to the scrolled V_2O_5 crystal making up the VONT, the reversibility of the insertion-removal redox process can potentially be improved compared to bulk materials, provided that intercalation sites for cations are not blocked by organic templates.[68,69]

In this work we show how high quality vanadium oxide nanotubes (VONTs) produced using an optimized synthetic protocol with amine-based structural templates, can be transformed into polycrystalline nanorods (poly-NRs) of V_2O_5 during annealing. We detail this process by monitoring both the inorganic and organic phase change and decomposition, respectively using IR spectroscopy, electron microscopy and X-ray diffraction analyzes. Through detailed electrochemical investigations of both VONTs and poly-NRs, we confirm that the removal of the amine-template from the VONTs and the thermally induced phase conversion to a polycrystalline structure improves specific capacity during discharging and charging as a Li-ion battery cathode material in the absence of a polymeric binder and conductive carbon additives in the electrode preparation. Thermal treatment of VONTs allows a specific structural transformation to poly-NRs during annealing which we classify and describe using electron microscopy, thermogravimetric analyzes and spectroscopic techniques. Based on structural analysis of pre- and post-lithiated VONTs and poly-NRs, we demonstrate that the heavy functionalization of VONTs by amine molecules can impede the intercalation of lithium ions, and that their removal and subsequent conversion to poly-NRs containing nanoscale crystallites results in a significant improvement in electrochemical characteristics.

*Electrochemical Society Fellow.
**Electrochemical Society Active Member.
[z]E-mail: c.odwyer@ucc.ie

Experimental

Vanadium oxide nanotubes were synthesized by hydrothermal treatment of a mixture of vanadium oxide xerogel and a primary amine, following usual procedures.[39,70,71] A nonylamine organic template was used in a molar ratio of xerogel to amine of 1:2, with 3 mL of ethanol added per gram of xerogel. This molar ratio of xerogel to amine was chosen as it was found to be the optimum ratio resulting in the highest yield of high quality VONTs.[72] The hydrothermal treatment resulted in a black suspension. This was then washed with ethanol and dried at room temperature using a Buchner funnel. The final product was a dry fluffy black powder consisting of VONTs. The poly-NRs for electrochemical testing were prepared by thermally treating VONT powder in a quartz glass furnace which was heated from room temperature to 600°C at 5°C min^{-1} in a nitrogen atmosphere.

Specimens for transmission electron microscopy (TEM) were prepared by dropping a suspension of VONTs onto a holey carbon grid. TEM analysis including bright field, dark field imaging, fast Fourier transforms (FFT) and electron diffraction was conducted using a JEOL JEM-2100F TEM operating at 200 kV. SEM analysis was performed using a Hitachi S-4800 at an accelerating voltage of 10 kV. Thermogravimetric analysis (TGA) was carried out using a Perkin Elmer TGA. VONT samples for TGA were placed in an alumina crucible and heated in 100°C increments to 600°C at a heating rate of 5°C min^{-1} and then cooled, in a nitrogen atmosphere. Fourier transform infrared spectroscopy (FTIR) was conducted on Perkin Elmer series 2000 apparatus in the region of 4000–650 cm^{-1}. For X-Ray Diffraction (XRD) analysis, a VONT/ethanol suspension was dried on a glass slide. In this way, the sample was measured as a thin film using an X'pert MRDpro Panalytical diffractometer with Cu Kα radiation (Cu Kα, $\lambda = 0.15418$ nm, operation voltage 40 kV, current 30 mA).

The electrochemical properties of bulk V_2O_5 powder, VONTs and poly-NRs were investigated using a three electrode cell. The cells were assembled inside a glove box under an argon atmosphere. The electrolyte consisted of a 1 mol dm^{-3} solution of lithium hexafluorophosphate salt in a 1:1 (v/v) mixture of ethylene carbonate in dimethyl carbonate. The working electrodes were prepared by dropping a sonicated mixture of the active material powder and ethanol on to a stainless steel foil substrate which was subsequently dried in a vacuum oven at 100°C for 2 hours. No additional conductive additives or binders were added to the various vanadium oxide working electrodes, allowing direct electrochemical examination of the various structures without complications from conductive additives and non-uniform mixtures. The counter and reference electrodes were pure lithium metal. Both working and counter electrodes had a geometric surface area of 1 cm^2. Galvanostatic discharge/charge tests were performed using a CH Instruments model 605B potentiostat/galvanostat in a potential window of 4.0 V–1.2 V with a constant current of ± 30 μA.

Results and Discussion

Synthesis of VONTs and conversion to polycrystalline nanorods.— Figure 1 shows representative SEM and TEM images of VONTs synthesized using a molar ratio of xerogel to amine of 1:2 with nonylamine used as the organic template. VONTs are traditionally synthesized using dodecylamine and hexadecylamine[43,73] which facilitate the scrolling of the layers of vanadium oxide during hydrothermal treatment.[42,71,74–76] High-quality VONTs were also successfully synthesized with a shorter nonylamine molecular template as shown in Fig. 1. Fig. 1a shows a plan view image of a bundle of VONTs where the open-ended, hollow-cored cylindrical shape can be seen. TEM was used to define the salient characteristic structural features of the VONTs. In Fig. 1b, the hollow core and the characteristic layered structure that appears to flank either side of the hollow center are visible. As typical of VONTs synthesized with other primary amines,[63] the resulting nonylamine nanotube walls consist of alternating bright and dark contrast fringes, as show in Fig. 1c. The dark, higher atomic weight fringes represent the vanadium oxide layers and the bright fringes represent the layers in which the interlayer nonylamine molecules are located.

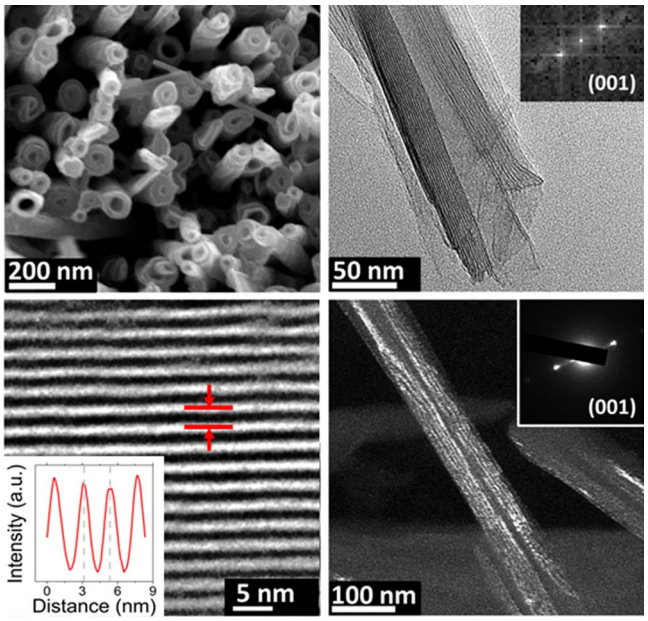

Figure 1. (a) SEM and (b) TEM images of VONTs synthesized using nonylamine in a molar ratio of xerogel to amine of 1:2, with an FFT inset. (c) HAADF TEM image of layered VONT walls showing the resulting interlayer spacing (dark features are V_2O_5, bright features are amines). (d) dark-field TEM image with electron diffraction pattern inset.

Although visually VONTs synthesized with nonylamine may look comparable to VONTs synthesized with the more commonly used dodecylamine and octadecylamine, VONTs synthesized with nonylamine have a reduced interlayer spacing between nanotube walls. The mean interlayer spacing for the VONTs in Fig. 1c was measured to be 2.17 nm, which is smaller than for VONTs grown using dodecylamine (~2.51 nm) and hexadecylamine (~2.98 nm).[72] The amine template is known to interdigitate as a bilayer between the sheets of vanadium oxide,[77,78] rather than forming a tilted, juxtaposed bilayer, resulting in a gallery spacing that is consistently less than twice the amine molecular length, for the majority of primary amines used in syntheses. Our previous systematic investigation of this effect confirmed that the degree of amine bilayer interdigitation increases with longer amine molecules.[79] This interlayer 'velcro' stabilizes the layered structure of the tubes during scrolling. Figure 1d shows a dark field TEM image of a typical VONT synthesized with nonylamine. The regions which appear bright in the dark field image are the vanadium-rich regions of the VONT. The FFT and electron diffraction insets in Fig. 1b and 1c respectively. The d-spacings for both techniques correspond to (001) reflections for orthorhombic V_2O_5. As-synthesized VONTs are functionalized with primary amines in order to maintain the structure comprising a single bilayer of V_2O_5 scrolled multiple times with a radius of curvature that defines the inner hollow core, and an interlayer spacing defined by the length of the amine template used and its interlayer structure.[39,43,62] The presence of nonylamine molecules may impede the intercalation of lithium ions within the VONTs which would have a detrimental effect on their electrochemical performance. It has previously been proposed that a high degree of organic molecular packing within the gallery spacing between the layers of VONT structures can negatively affect lithium insertion and thus cathode performance of as-synthesized VONTs.[42,63] Therefore, we investigated the removal of the organic template while still maintaining the advantageous nano-scale dimensions of the material. In order to do this, thermogravimetric analysis of the VONTs was carried out where

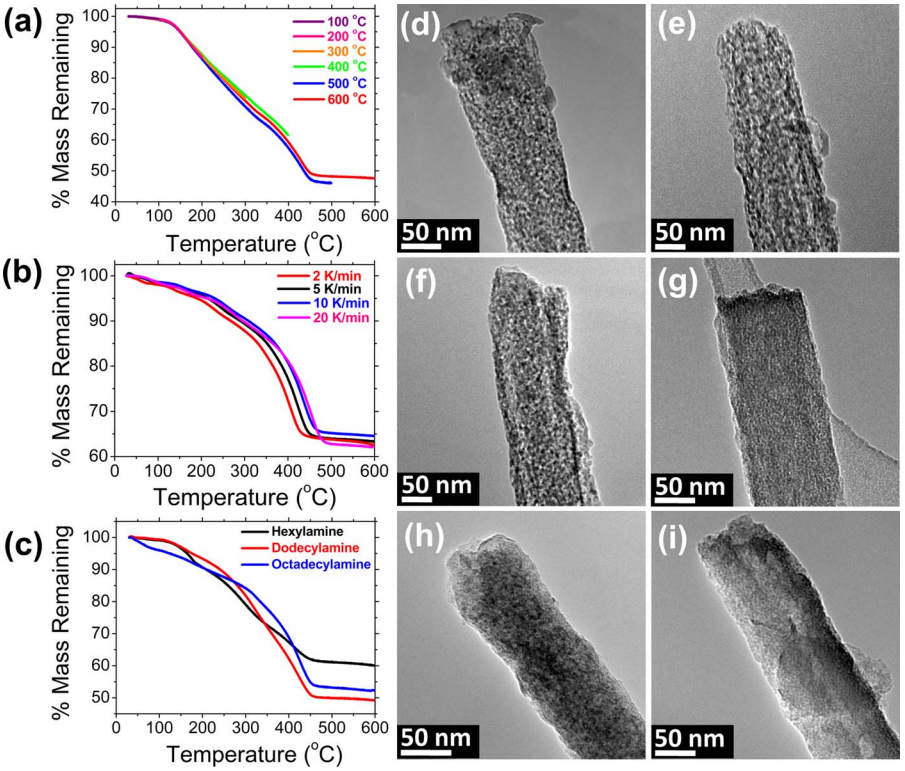

Figure 2. (a) TGA curves for nonylamine VONT samples (a) heated to temperatures ranging from 100°C to 600°C at a heating rate of 5°C/min and (b) annealed at different heating rates. (c) TGA curves for VONTs synthesized with different amines. TEM images of nonylamine-contaiing VONTs converted to poly-NRs at 600°C at (d) 2°C/min, (e) 10°C/min and (f) 20°C/min. TEM images of resulting poly-NRs annealed to 600°C which were prepared with (g) hexylamine, (h) dodecylamine and (i) octadecylamine.

samples of nonylamine 2:1 xerogel VONTs were heated to a series of different temperatures (100°C to 600°C in 100°C increments) in a nitrogen atmosphere.

Figure 2a shows the resulting TGA mass loss curves for nonylamine 2:1 xerogel VONT samples, annealed at a constant heating rate of 5°C/min. As can be seen in Fig. 2a, less than 1% (0.82%) mass is lost when the VONTs are heated to 100°C. Significant mass losses begin to occur when the VONTs are heated above ∼120°C as indicated by the knee in curves. The initial mass losses are most likely due to the removal of physisorbed and chemisorbed water present within the VONTs. After this region, there is an almost linear decrease in mass loss as temperature increases until the VONTs reach a temperature of ∼450°C. At this stage ∼45% of the mass of the VONTs has been lost and the curves begin to level off, implying the total amount of material which can be removed from the VONTs through thermal annealing has already been removed. The mass losses in this region are due to the removal of amines which functionalize the walls of the nanotubes.[78] The boiling point of nonylamine is ∼201°C, hence a higher temperature is needed to overcome stronger bonding and interaction forces of the interdigitated and confined, bound interlayer molecules. Figure 2b shows the resulting mass loss curves for the same VONTs which were annealed at different heating rates. The mass loss for each sample leveled off and remains relatively consistent between 465°C and 500°C. At the higher heating rate (20°C/min), this mass removal process leveled off at ∼490°C, which we surmize is due to a time-dependent desorption rate for the amine molecules on the vanadium oxide; lower heating rates require lower upper temperatures for an equivalent organic mass removal over a similar time. Figures 2d, 2e and 2f show TEM images of VONTs converted to poly-NRs after annealing to 600°C at 2°C/min, 10°C/min and 20°C/min respectively. The nanostructures produced at these heating rates were all poly-NRs with grain sizes comparable to the poly-NRs which were annealed with a heating rate of 5 K/min as shown in Fig. 3f. From these images it is clear that the transition from VONT to poly-NR occurs irrespective of their heating rate for the range of rates investigated.

VONTs synthesized with different primary amines have different interlayer spacings. VONTs which were prepared with amines other than nonylamine were also annealed to 600°C, to determine if VONTs which initially have different interlayer spacings would form comparable poly-NR structures. Figure 2c shows the mass loss curves for VONTs synthesized with different amine molecules. The three different amines which were used were hexylamine (6 C–C), dodecylamine (12 C–C) and octadecylamine (18 C–C). Hexylamine is the shortest and lightest amine of the three; consequently VONTs synthesized with hexylamine underwent the least amount of mass loss (∼35%) when annealed to 600°C. VONTs synthesized with dodecylamine and octadecylamine lost a higher percentage of their mass, ∼50% and ∼45% respectively. It is clear that all three samples undergo a similar transition as VONTs synthesized with nonylamine during annealing, with the three mass loss curves all leveling off at ∼450°C. Figures 2g, 2h and 2i show TEM images of VONTs synthesized with hexylamine, dodecylamine and octadecylamine respectively, after annealing. These images show that these VONTs underwent a similar structural transition from VONT to poly-NR. From these observations, it was characteristically found that the transition from VONT to poly-NR occurs (i) irrespective of the heating rate and (ii) irrespective of the length of the primary amine chain. The most important parameter is that VONTs are annealed to 600°C in a nitrogen atmosphere in order to completely decompose and remove the organic phase and recrystallize the inorganic phase.

It can be expected that the removal of amine molecules will largely affect the structure of the VONTs as they are the structure maintaining template that facilitate VONT formation. Microscopy examination using TEM of VONTs heated in 100°C increments from 100°C to 600°C, shown in Fig. 3 shows that thermal decomposition of the organic template and the scrolled vanadium oxide sheets above the crystallization temperature for amorphous vanadium oxide results in a drastic change in the morphology of the VONT. The resulting structure maintains a similar aspect ratio to the original nanotube, but now consists of grains or crystallites throughout the rod-like structure.

As synthesized VONTs have three main features: the tube openings, the hollow core and the multilayer walls.[44] VONTs which have been heated to 100°C, 200°C and 300°C in a nitrogen atmosphere clearly retain all three of these features as can be seen in Fig. 3a - 3c. The hollow core is no longer visible for VONTs heated to 400°C and above, and the ED pattern shows the presence of an amorphous

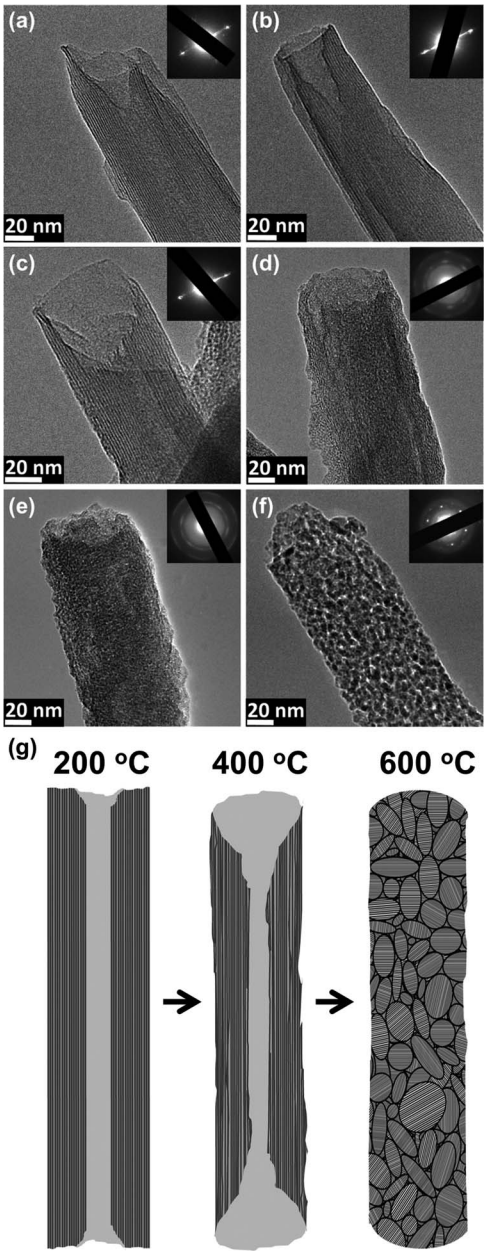

Figure 3. TEM images of VONTs annealed to various temperatures (a) 100°C, (b) 200°C, (c) 300°C, (d) 400°C, (e) 500°C, (f) 600°C. The inset show corresponding electron diffraction patterns showing the conversion from parallel crystalline layers to polycrystalline V_2O_5 formation. (g) Schematic representation of the transition from a highly ordered as-synthesized VONT to a disordered VONT, and eventually to a polycrystalline nanorod (poly-NR) as temperature increases.

diffuse ring with arced diffraction spots consistent with rotated crystallites of V_2O_5. There are regions in the VONTs heated to 400°C and 500°C which still exhibit the characteristic multilayer walls as can be seen in Fig. 3d and 3e. VONTs heated to these temperatures also still maintain definite open tube endings. The most significant structural change occurs when the VONTs are heated to 600°C. After thermal treatment, the order in their structure (layers with a consistent interlayer spacing) is lost due to the removal of the nonylamine molecules and recrystallization of the vanadium oxide into poly-NRs. The definite tube opening is no longer visible and the multilayer walls have been converted to a high density of granular features. The crystallization is confirmed by a reduction in the intensity and diffuse nature of the amorphous ring, and the presence of dominant V_2O_5

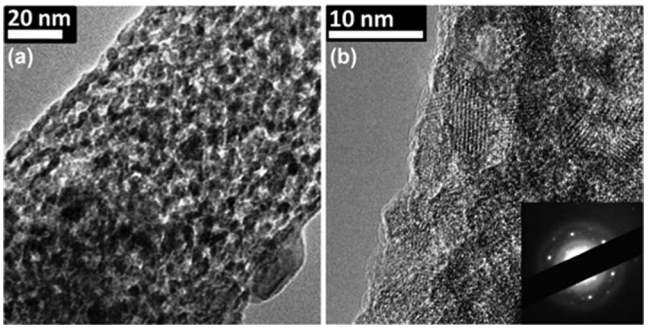

Figure 4. (a) TEM image of nonylamine 2:1 xerogel VONTs after thermal treatment to 600°C, (b) TEM image of the polycrystalline nature of the poly-NR showing 5–10 nm grain sizes within the structure. (Inset) Selected area electron diffraction pattern of nanocrystalline grains.

reflections from equi-axed crystallites together with reflections from crystals oriented along a different zone axis.

After annealing, VONTs recrystallize into vanadium oxide poly-NRs. The polycrystalline structure of poly-NRs can be seen in Fig. 4a, where each of the constituent grains is a nanoscale crystallite of vanadium pentoxide. This is further illustrated in Fig. 4b where the individual grain boundaries for each of the crystallites can be seen. The electron diffraction pattern inset in Fig. 3c confirms that the nanocrystals are orientated independently of each other. The interplanar spacing of the poly-NRs was measured to be 0.22 nm which corresponds to the d-spacing of (002) plane of bulk V_2O_5 powder.

The proposed mechanism for the formation of poly-NRs is shown in Fig. 3g. Initially as synthesized VONTs are pristine nanotubes with well-defined tube opening and layered walls. As VONTs are heated to 300°C the tube openings are observed to widen and the walls of the VONT become disordered and begin to lose their parallel and straight structure. When VONTs are further heated to 600°C there is a structural change from a disordered VONT to a poly-NR. Poly-NRs consist of a granular agglomeration of nanocrystals of vanadium pentoxide, and remarkably, they still maintain similar overall dimensions to the VONTs prior to annealing. This change in physical structure is facilitated by the removal of crystal water and the structure-maintaining amine template, and recrystallization of layered vanadium oxide into individual nanocrystals. Heating up to 650°C however, resulted in sintering of the nanocrystals into slightly large crystals on the outer surface of a less uniform poly-NR structure (see supplementary materials, Fig. S1). The nano crystallites which make up the poly-NR structure coalesce to form larger crystallites.

In order to investigate the thermal decomposition of VONTs to poly-NRs, FTIR spectra were acquired for VONTs at each stage of the heating process. The FTIR spectra for orthorhombic bulk V_2O_5, as-synthesized VONTs (not heated) and VONT samples heated in a temperature range from 100°C to 600°C are shown in Fig. 5. The spectra show that the vibrational contribution of the intercalated amines markedly change during heating.

The absorption at 720–750 cm^{-1} is attributed to lattice vibration of vanadium oxide (V-O^-). As can be seen in Fig. 5a, a significant difference in the V-O^- vibrations of the VONT samples is observed as the annealing temperature is increased. The spectra are rich in absorption peaks from V-O-V, V-O, and V= O/V-O^-, especially for ordered VONTs up to 100°C, where Fig. 5a confirms the strong absorption from the reduced vanadyl bond in VONTs compared to bulk. The vanadyl (V=O) peak is typically observed between 950–1100 cm^{-1} in bulk V_2O_5; its frequency reduction to wavenumbers <1000 cm^{-1} is characteristic of an increased V^{4+} quanitity (reduced bond strength), which is a characteristic of VONTs.[80] As the annealing temperature is increased above 100°C, the VONT V=O vibrational signature changes and becomes similar to that of crystalline V_2O_5, but is found to broaden, implying that a disorder of the VONT structure occurs.[81] The peaks observed between 1360–1560 cm^{-1} and

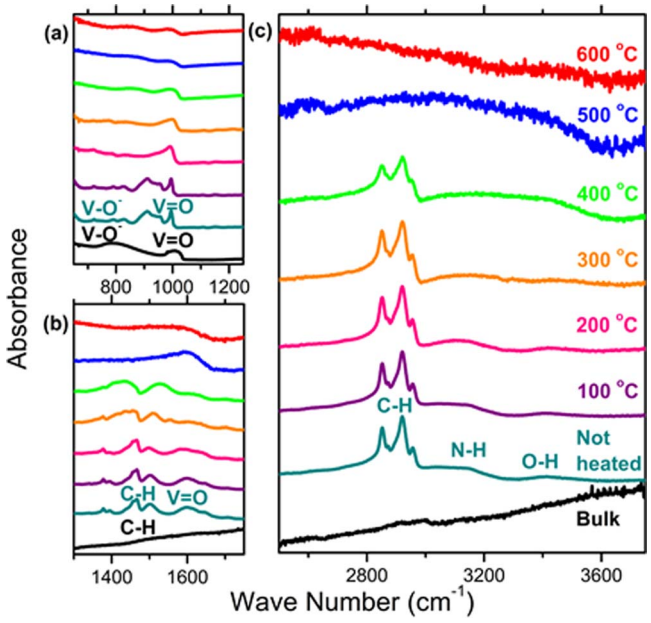

Figure 5. FTIR spectra for bulk V_2O_5 powder, as synthesized VONTs (not heated) and VONTs heated to temperatures ranging from 100°C to 600°C.

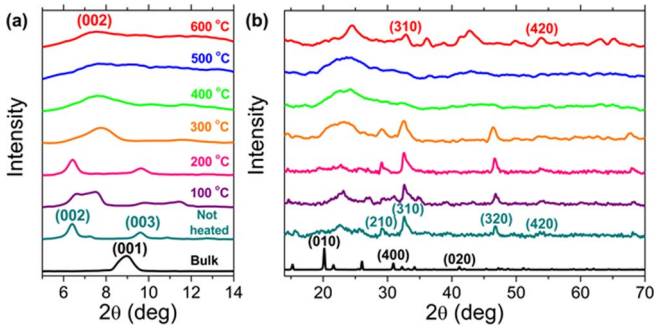

Figure 6. XRD comparison (a) (00*l*) reflections (b) (*hk*0) reflections from orthorhombic V_2O_5 crystalline powder (JCPDS 09–0387), as synthesized VONTs and those heated in 100°C increments.

2850–2930 cm^{-1}, in Fig. 5b are due to C-H bending and asymmetric and symmetric stretching vibrations, respectively.[31,78,82] The broad band beginning at 3040 cm^{-1} is assigned to ammonium ions implying that the NH_2 head groups of the amine molecules are present in the vanadium oxide layers as NH_3^+ groups. Another broad band from 3300 cm^{-1} to 3650 cm^{-1} is attributed to the stretching and bending modes of O-H vibrations. Both of these bands are not found, as expected, in the spectra from bulk V_2O_5 powder, but are quite clear in the IR absorbance from the VONTs due to amine molecules and water (in the form OH groups and crystal water). The symmetric and asymmetric CH_2 and CH_3 vibrations (2700–3000 cm^{-1}) reduce in intensity with increasing temperature and are no longer visible above 400°C indicating a decomposition of the alkyl chain and methyl tail groups. From comparison with crystalline powder V_2O_5 and poly-NRs, the absence of both C-H and the majority of N-H vibrations confirm the successful removal of the amine template, while the inorganic phase decomposes from a single molecule-thick scrolled sheet to a polycrystalline nanorod.

Spectroscopic measurements do show that some of the electrostatically bound, oxidized amino head groups (NH_3^+) still remain after thermal treatment. There is evidence for this from the vibrational response between 1610–1620 cm^{-1} associated with an O-H vibration, which can be seen in the spectra for VONTs and poly-NRs, but are not found in the bulk V_2O_5 spectra (Fig. 5c). During the initial aging stage in the preparation of the VONTs, amines are hydrolyzed to form ammonium ions and hydroxide ions. The resulting hydroxide ions reduce the V=O bond present in the V_2O_5 molecule to form (V-OH) and ($V\text{-}O^-$) bonds[78] and in this manner the vanadium becomes six-coordinated (comprising VO_5 subunits making up V_2O_5) while still retaining a predominantly pentavalent oxidation state.[83] Overall, the key vibrational signatures from several important functional groups related to the intercalated organic template are effectively removed only after heating above 400°C. This is fully consistent with heating rate-dependent TGA investigations presented in Fig. 2 and shows that the confined geometry and strong intermolecular forces within VONTs require temperatures greater than the boiling point of the respective amines (independent of heating rate) to fully remove them from the VONT structure.

Significantly, the FTIR spectrum obtained for poly-NRs is very similar to that of bulk crystalline V_2O_5 powder, as shown in Fig. 5. The vanadyl (V=O) peaks for both of these samples are very similar. Likewise the vibrational contribution due to the intercalation of amine molecules is not observed for either of these samples. The FTIR spectra indicate that there is a conversion from disordered V_2O_5 to polycrystalline V_2O_5 after thermal treatment to 600°C. This suggests that the nanocrystallites which make up the poly-NRs are structurally very similar to the bulk orthorhombic V_2O_5 precursor. The structural similarities between these two samples will be further discussed through the analysis of their X-ray diffraction patterns. The polymorphism in the inorganic phase of the VONTs was also monitored using XRD. The XRD patterns of bulk V_2O_5, as synthesized VONTs, and VONTs heated in 100°C increments are shown in Fig. 6. Figures 6a and 6b show two characteristic regions in the diffraction patterns. The low angle region in Fig. 6a show (00*l*) Bragg reflection peaks of VONTs annealed to a series of different temperatures including diffraction analysis of as-synthesized VONTs and from bulk V_2O_5 powder. The (002) and (003) peaks consistent with a periodic layered structure[84–87] are still observed for VONT samples heated to 200°C. The (002) peak for VONT samples heated above 200°C is shifted from ~6.4° to ~7.6° indicating a reduction in the interlayer distance, and the (003) reflection is no longer present. This confirms that there is a structural rearrangement of layers comprising the VONT structure as they are annealed to high temperatures. As these low angle reflections represent the consistency in layering within the VONT, their absence infers a reduction in this order, consistent with the TEM evidence in Fig. 3. The absence of obvious reflections at low angles in Fig. 6a definitively shows that the layering within the VONTs no longer exists after heating to 600°C.

The second region shown in Fig. 6b comprises (*hk*0) reflections, characteristic of the crystal structure of the V_2O_5.[39,42,70,71,88,89] These reflections in VONTs represent diffraction from the crystalline material comprising the layers themselves. A characteristic of curved single crystals is a 'Fano-type' lineshape;[39] in VONTs, this is indicative of the high structural order of a scrolled VONT. A series of 'Fano-type' peaks were observed in the diffraction pattern for as-synthesized VONTs, including (210), (310), (320) and (420) peaks. This series of peaks are also present in the diffraction patterns of VONTs annealed up to and including 300°C. However, as the VONTs are annealed to higher temperatures, these peaks begin to broaden due to a reduction in crystalline order within the scrolls making up the VONT. This has also been verified through TEM imaging the VONTs as shown in Fig. 4, and is consistent with a removal of the structure-maintaining organic template as determined by FTIR measurements in Fig. 5. VONTs heated to from 400°C to 600°C do not exhibit the same lineshapes which is a clear indication of the collapse of the consistent degree of curvature within the scrolled sheets making up the tubular structure. The (110) peak is present for all VONT samples; the width of the peak increases as the temperature of the VONTs increases, which is consistent with a reduction in order within the VONT, and the presence of small crystallites within the structure. The transition observed in the XRD patterns for VONTs converted to poly-NRs at 600°C is consistent with microscopy and IR data discussed earlier. The XRD

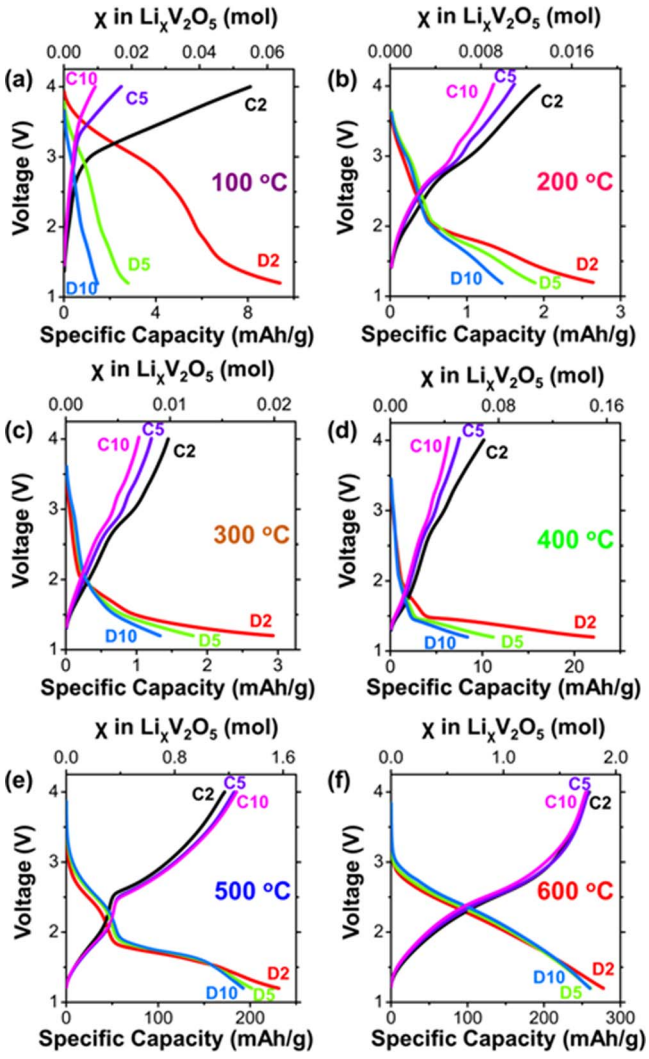

Figure 7. 2nd, 5th and 10th discharge curves for VONT samples heated to (a) 100°C, (b) 200°C, (c) 300°C, (d) 400°C, (e) 500°C, (f) 600°C.

pattern for poly-NRs exhibits numerous reflections identical to those found for bulk V_2O_5, but at a higher angle, which is consistent with the effects of reduced size of an identical crystal structure.

Lithium insertion and removal in poly-NR battery electrodes.— The cycling performance of VONT samples heated in 100°C increments is shown in Fig. 7. The results shown are for the 2nd, 5th and 10th cycles. The shape of the discharge/charge curves offer an insight into the lithium insertion mechanism which occurs for each sample. The first discharge curves for orthorhombic V_2O_5 and VONT samples heated to 300 and 600°C are shown in Fig. S2. It is clear that the phase transitions which are characteristic of lithium intercalation into bulk V_2O_5, smoothen for VONTs and are not observed for poly-NRs. The number of moles of lithium inserted into VONT samples heated from 100–400°C inclusively does not exceed ≈0.16 mol, hence, in accordance with previous studies,[90,91] the phase transition which can be seen in the discharge/charge curves (Fig. 7a - 7d) for these samples corresponds to the α-phase ($\chi \geq 0.01$). It has been reported that for an orthorhombic bulk V_2O_5 sample discharged to ≈1.6 V, approximately 3.0 moles of lithium can be inserted, resulting in the formation of the irreversible ω-phase[92] leading to the theoretical maximum capacity of ∼440 mAh/g. These samples were discharged to a lower potential of 1.2 V, however for VONT samples heated from 100–400°C only ≈ 0.16 moles of lithium can be successfully inserted. This supports the evidence presented earlier that the amine molecules occupying van der Waals spaces between the vanadium oxide layers block Li ion intercalation sites at the oxide surface and consequently impede their insertion. When VONTs are heated to 500 and 600°C, an efficient removal of amines is possible as indicated from TGA and FTIR analysis. The resulting poly-NR structures were able to host a greater amount of lithium in structures comprising a higher density of nanoscale crystallites and grain boundaries.

The discharge/charge curves for the VONT sample heated to 500°C show 3 phases transitions associated with the intercalation of Li ions; the α-phase ($\chi \geq 0.01$), the ϵ-phase ($\chi \approx 0.35$) and the δ-phase ($\chi \approx 1.0$). After the 2nd discharge ≈1.57 mol of Li ions were inserted into the poly-NR sample and after the 2nd charge 1.17 mol were removed. This indicates that while not all of the lithium is being successfully removed during charging, the sample heated to 500°C does have significantly improved reversibility when compared to VONT samples heated from 100 to 400°C. When VONTs are heated to 600°C an even greater content of lithium can be inserted into the poly-NR structure (≈1.8 mol). This is most likely due to the 600°C sample having fewer amines remaining than poly-NRs formed at 500°C. Interestingly the discharge/ charge curves for the 600°C sample do not show any discrete phase transitions, instead they are smooth curves. This is typically indicative of an amorphous material. TEM imaging, electron diffraction and XRD analysis all prove that the resulting structures for the sample heated to 600°C are indeed polycrystalline on the nanoscale (2–10 nm crystallites). The overall poly-NR structure responds electrochemically as an amorphous-like phase undergoing lithiation, i.e. without discrete voltage steps in the discharge curve. Similar smooth cycling curves were reported for vanadium oxide xerogels which were heated to 300°C.[93] There is also an improvement in the reversibility of Li ion insertion/removal with ≈1.8 mol being inserted and removed after the 5th and 10th discharge and charge.

The specific capacity values obtained from the 2nd to the 10th cycle for VONTs that were prepared by heating in 100°C increments, are also shown in Fig. 7 and summarized in Fig. 8a. From Fig. 8a it is clear that annealing VONTs to high temperatures (≥500°C) has a significant effect on their electrochemical performance.[63,94–96] VONT samples heated to 100, 200, 300 and 400°C all suffered from severe capacity fading. The percentage specific capacity losses for these samples from the 2nd to the 10th were ≈84, 45, 55 and 62% respectively. However, when VONT samples were heated to temperatures higher than 400°C, there was a considerable improvement in the initial specific capacity as well as in the cycling performance. The specific capacities for poly-NRs formed at 500 and 600°C after the second discharge were ≈231 and 278 mAh/g respectively. After the 10th cycle these values slightly decreased to ≈193 and 260 mAh/g respectively. These values corresponding to percentage specific capacity losses for poly-NRs formed at 500 and 600°C of ≈17 and 6%, respectively. The poly-NRs demonstrated high coulombic efficiency, with the coulombic efficiency for the VONT sample heated to 600°C being ≈98% for the first 10 cycles (see supplementary materials Fig. S3). The energy densities for VONT samples after annealing are shown in Fig. 8b, calculated based on a voltage window of 4.0–1.2 V. In this potential window, no electrolyte decomposition occurs that affects that stable coulometric efficiency of this electrode material in a carbonate-based electrolyte. The calculated values for VONT samples heated to 100, 200 and 300°C were ∼24.1, 6.3 and 6.8 W h kg^{-1} respectively, as shown in Fig. 6.14. When VONTs were heated to 400°C the energy density was increased to 50.3 W h kg^{-1}. The energy densities for poly-NRs formed at 500 and 600°C were also significantly increased with values corresponding to 578.5 and 699.2 W h kg^{-1}, respectively. The calculated energy density values indicate that VONT samples heated above 500°C exhibit a significant improvement in electrochemical performance over as-synthesized VONTs.

Galvanostatic cycling of VONT samples heated in the range of 100–400°C demonstrates that amine-templated VONTs suffer from severe capacity fading and miniscule specific capacities. The poor performance of VONT samples heated in the range of 100–400°C is attributed to the presence of the surface-capping amines. The

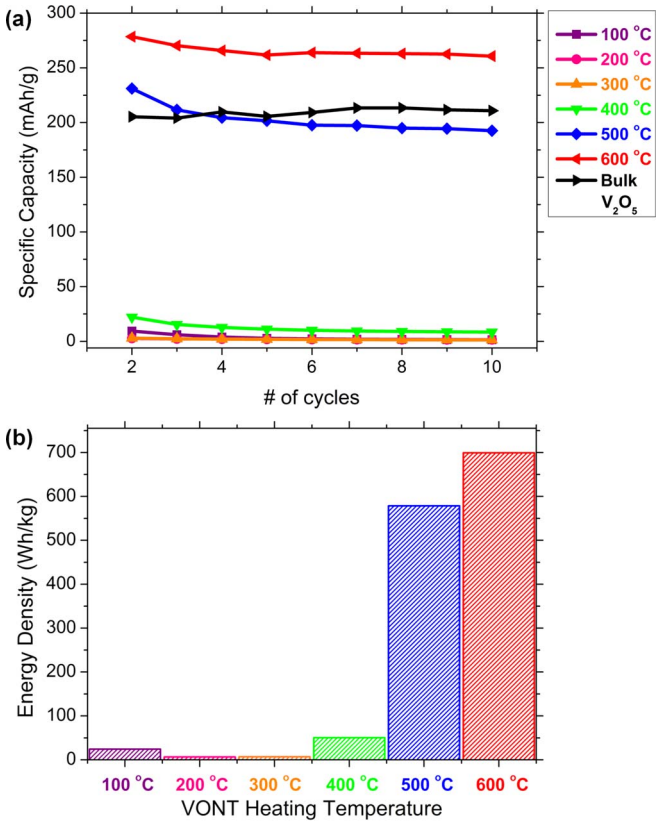

Figure 8. (a) Discharge capacities of VONT samples heated to temperatures in the range of 100°C–600°C. Each sample was cycled in a potential window of 4.0–1.2 V with a constant current of 30 μA, (b) Energy density values for thermally treated VONT samples after the 2nd discharge.

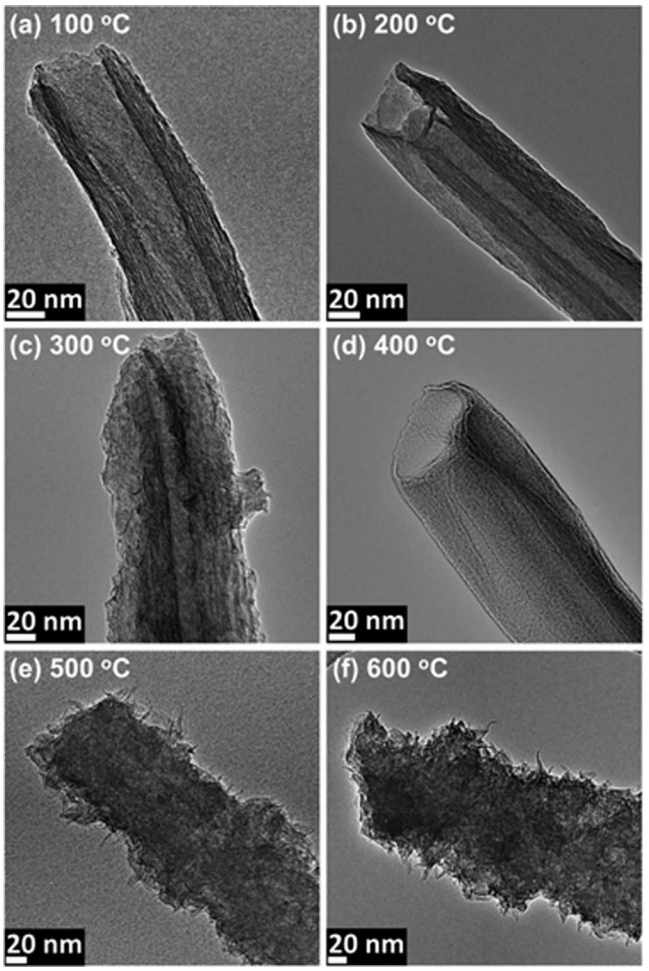

Figure 9. TEM images of thermally treated VONTs after 10 cycles at ± 30 μA in a potential window of 4.0–1.2 V. (a) 100°C, (b) 200°C, (c) 300°C, (d) 400°C, (e) 500°C, (f) 600°C.

partial removal of amines from VONTs has no significant effect on the cycling performance of the VONTs. The poly-NR sample heated to 500°C has specific capacities similar to orthorhombic V_2O_5 powder over the first 10 cycles, however the sample heated to 600°C has significantly higher specific capacity values than both of those samples, as seen in Fig. 8a.

After galvanostatic cycling, each VONT sample was imaged by TEM. The resulting images are shown in Fig. 9. After 10 cycles, the VONT samples heated from 100–300°C, maintain the characteristic nanotube morphology as can be seen in Fig. 9a – 9c. In fact, when compared to Fig. 3a – 3c there is little evidence of any visible changes to the VONT structures, the hollow core, layer walls and open ends are all well preserved. The VONT sample heated to 400°C also appears quite similar before and after cycling. The distinct tube opening and portions of layered walls can be seen along the length of the VONT, as shown in Fig. 9d. The similarity in the appearance of VONTs heated in a temperature range from 100°C to 400°C before and after cycling suggests that the structure maintaining amine molecules are still present and have not been exchanged for Li ions during cycling. There is also evidence of this in the analysis of the intercalation of lithium ions into thermally treated VONTs. The low amounts of lithium which were successfully intercalated into VONT samples heated from 100°C to 400°C, shown in Fig. 7 also suggest that amine molecules are not exchanged with lithium ions. It appears as though the electrostatic bond between the amine NH_2 head group and vanadium is too strong for a partial ion exchange to occur with Li ions during cycling. This suggests that for VONTs containing amines, low amounts of lithium ions are inserted where intercalation sites are not already occupied and hence the structure of these VONTs is not significantly altered as a result of cycling. The poly-NR samples which were heated to 500°C and 600°C undergo a significant structural change as a result of cycling, as can be seen in Fig. 9e and 9f when compared to Fig. 3e and 3f. After cycling the nanocrystalline grains that make up the poly-NRs expand due to the repeated insertion and removal of Li ions. Consequently the nanocrystalline grains along the outer edges of the poly-NRS are observed as nanorod-type structures with much sharper edges. These flakes contain layers of vanadium oxide (see supplementary materials, Fig. S4). Recent investigations using bicontinuous hierarchical $Li_3V_2(PO_4)_3$ mesoporous nanowires, which are also composed of nanoscale grains of materials, show how some variants of polycrystalline materials are beneficial for long term cycling.[97]

Conclusions

As synthesized VONTs are heavily functionalized with nonylamine molecules during their synthesis, and occupy the surface sites for cation intercalation. Through thermogravimetric analysis it was verified that the organic amine template can be removed from the VONTs upon heating to 600°C, verified by FTIR, TEM and XRD analysis of VONTs heated from 100°C to 600°C illustrate the gradual change in the morphology as the amine molecules are being removed. Microscopy and spectroscopy analyses demonstrate the conversion from scrolled VONTs to polycrystalline vanadium oxide nanorods. The resulting nanorods maintain similar original aspect ratio, width and length of the original VONTs.

We also define the limitations of VONTs due to their functionalization, which has implications for other nanoparticle synthetic systems

with shape-influencing ligands on facets amenable to Li ion insertion, or structural organic templates in layered or solvent-exfoliated material systems. Galvanostatic cycling of VONT samples heated in 100°C increments demonstrated that VONTs containing amines suffer from severe capacity fading. The specific capacity values obtained for VONTs samples heated in the temperature range from 100°C to 400°C were miniscule compared to values obtained with bulk V_2O_5.

When VONT samples are heated to 500 and 600°C there is a significant increase in the initial specific capacity values as well improved cycling stability. In a potential window of 4.0–1.2 V drawing 30 μA (C/30), the nanorods show improved specific capacities of ∼280 mAh g^{-1} with a modest 6% capacity fade compared to ∼8 mAh g^{-1} with 62% capacity fade for the VONTs. This improvement is shown by TGA, TEM, FTIR, XRD analysis and galvanostatic cycling, to be due to the presence of amine molecules at the intercalation sites. Their removal significantly improves cathode performance. The cathode material also enhances gravimetric energy densities (≈ 700 W h kg^{-1}) compared to composites of the same overall weight, without conductive carbon additives nor polymeric binders.

Supplementary Materials

Details of the effects of heating VONTs sample to 650°C and the coulombic efficiencies and energy densities achieved for VONT samples heated in 100°C increments are provided.

Acknowledgments

This publication has emanated from research conducted with the financial support of the Charles Parsons Initiative and Science Foundation Ireland (SFI) under grant No. 06/CP/E007. Part of this work was conducted under the framework of the INSPIRE program, funded by the Irish Government's Program for Research in Third Level Institutions, Cycle 4, National Development Plan 2007–2013. COD acknowledges support from Science Foundation Ireland under award no. 07/SK/B1232a, the UCC Strategic Research Fund, and from the Irish Research Council New Foundations Award.

References

1. J. M. Tarascon and M. Armand, *Nature*, **414**, 359 (2001).
2. P. G. Bruce, B. Scrosati, and J.-M. Tarascon, *Angewandte Chemie International Edition*, **47**, 2930 (2008).
3. A. Stein, *Nat. Nanotechnol.*, **6**, 262 (2011).
4. J. B. Goodenough and Y. Kim, *Chem. Mater.*, **22**, 587 (2009).
5. M. Osiak, H. Geaney, E. Armstrong, and C. O'Dwyer, *J. Mater. Chem. A* (2014).
6. A. S. Arico, P. Bruce, B. Scrosati, J. M. Tarascon, and W. V. Schalkwijk, *Nat. Mater.*, **4**, 366 (2005).
7. C. Liu, F. Li, L.-P. Ma, and H.-M. Cheng, *Adv. Mater.*, **22**, E28 (2010).
8. S. Wang, Z. Lu, D. Wang, C. Li, C. Chen, and Y. Yin, *J. Mater. Chem.*, **21**, 6365 (2011).
9. M. J. Armstrong, C. O'Dwyer, W. J. Macklin, and J. D. Holmes, *Nano Res.*, **7**, 1 (2014).
10. J.-i. Hahm and C. M. Lieber, *Nano Letters*, **4**, 51 (2003).
11. P. Alivisatos, *Nat Biotech*, **22**, 47 (2004).
12. M. Darder, P. Aranda, and E. Ruiz-Hitzky, *Adv. Mater.*, **19**, 1309 (2007).
13. N. Lee and T. Hyeon, *Chemical Society Reviews*, **41**, 2575 (2012).
14. C. Bae, H. Yoo, S. Kim, K. Lee, J. Kim, M. M. Sung, and H. Shin, *Chem. Mater.*, **20**, 756 (2008).
15. S. B. Lee, D. T. Mitchell, L. Trofin, T. K. Nevanen, H. Söderlund, and C. R. Martin, *Science*, **296**, 2198 (2002).
16. R. Fan, R. Karnik, M. Yue, D. Li, A. Majumdar, and P. Yang, *Nano Letters*, **5**, 1633 (2005).
17. J. Qiu, F. Zhuge, X. Li, X. Gao, X. Gan, L. Li, B. Weng, Z. Shi, and Y.-H. Hwang, *J. Mater. Chem.*, **22**, 3549 (2012).
18. P. Liu, H. Zhang, H. Liu, Y. Wang, X. Yao, G. Zhu, S. Zhang, and H. Zhao, *J. Am. Chem. Soc.*, **133**, 19032 (2011).
19. H. T. Ng, J. Han, T. Yamada, P. Nguyen, Y. P. Chen, and M. Meyyappan, *Nano Letters*, **4**, 1247 (2004).
20. Y. Cui, Z. Zhong, D. Wang, W. U. Wang, and C. M. Lieber, *Nano Letters*, **3**, 149 (2003).
21. C. K. Chan, H. Peng, G. Liu, K. McIlwrath, X. F. Zhang, R. A. Huggins, and Y. Cui, *Nat Nano*, **3**, 31 (2008).
22. G. Che, B. B. Lakshmi, E. R. Fisher, and C. R. Martin, *Nature*, **393**, 346 (1998).
23. C. N. R. Rao and M. Nath, *Dalton Transactions*, **0**, 1 (2003).
24. B. A. Korgel, *J. Phys. Chem. Lett.*, **5**, 749 (2014).
25. I. E. Wachs and B. M. Weckhuysen, *Applied Catalysis A: General*, **157**, 67 (1997).
26. G. C. Bond and S. F. Tahir, *Applied Catalysis*, **71**, 1 (1991).
27. R. André, F. Natálio, M. Humanes, J. Leppin, K. Heinze, R. Wever, H. C. Schröder, W. E. Müller, and W. Tremel, *Advanced Functional Materials*, **21**, 501 (2011).
28. G. Gu, M. Schmid, P.-W. Chiu, A. Minett, J. Fraysse, G.-T. Kim, S. Roth, M. Kozlov, E. Muñoz, and R. H. Baughman, *Nature materials*, **2**, 316 (2003).
29. B. Azambre and M. Hudson, *Mater. Lett.*, **57**, 3005 (2003).
30. B. Azambre, M. Hudson, and O. Heintz, *J. Mater. Chem.*, **13**, 385 (2003).
31. J. Liu, X. Wang, Q. Peng, and Y. Li, *Adv. Mater.*, **17**, 764 (2005).
32. G. Eranna, B. C. Joshi, D. P. Runthala, and R. P. Gupta, *Critical Reviews in Solid State and Materials Sciences*, **29**, 111 (2004).
33. F. Natalio, R. André, S. A. Pihan, M. Humanes, R. Wever, and W. Tremel, *J. Mater. Chem.*, **21**, 11923 (2011).
34. S. Myung, M. Lee, G. T. Kim, J. S. Ha, and S. Hong, *Adv. Mater.*, **17**, 2361 (2005).
35. N. Pinna, U. Wild, J. Urban, and R. Schlögl, *Adv. Mater.*, **15**, 329 (2003).
36. S. Webster, R. Czerw, R. Nesper, J. DiMaio, J.-F. Xu, J. Ballato, and D. Carroll, *Journal of Nanoscience and Nanotechnology*, **4**, 260 (2004).
37. J. Cao, J. Choi, J. Musfeldt, S. Lutta, and M. Whittingham, *Chem. Mater.*, **16**, 731 (2004).
38. A. V. Grigorieva, A. B. Tarasov, E. A. Goodilin, S. M. Badalyan, M. N. Rumyantseva, A. M. Gaskov, A. Birkner, and Y. D. Tretyakov, *Mendeleev Communications*, **18**, 6 (2008).
39. F. Krumeich, H. J. Muhr, M. Niederberger, F. Bieri, B. Schnyder, and R. Nesper, *J. Am. Chem. Soc.*, **121**, 8324 (1999).
40. F. Sediri, F. Touati, and N. Gharbi, *Mater. Lett.*, **61**, 1946 (2007).
41. J. Livage, *Chem. Mater.*, **3**, 578 (1991).
42. M. Niederberger, H.-J. Muhr, F. Krumeich, F. Bieri, D. Günther, and R. Nesper, *Chem. Mater.*, **12**, 1995 (2000).
43. M. E. Spahr, P. Bitterli, R. Nesper, M. Müller, F. Krumeich, and H. U. Nissen, *Angew. Chem. Int. Edit.*, **37**, 1263 (1998).
44. G. R. Patzke, F. Krumeich, and R. Nesper, *Angew. Chem. Int. Edit.*, **41**, 2446 (2002).
45. A. M. Cao, J. S. Hu, H. P. Liang, and L. J. Wan, *Angew. Chem. Int. Edit.*, **44**, 4391 (2005).
46. J. Muster, G. T. Kim, V. Krstić, J. G. Park, Y. W. Park, S. Roth, and M. Burghard, *Adv. Mater.*, **12**, 420 (2000).
47. S. Nordlinder, J. Lindgren, T. Gustafsson, and K. Edström, *J. Electrochem. Soc.*, **150**, E280 (2003).
48. J.-F. Xu, R. Czerw, S. Webster, D. Carroll, J. Ballato, and R. Nesper, *Appl. Phys. Lett.*, **81**, 1711 (2002).
49. L. Krusin-Elbaum, D. Newns, H. Zeng, V. Derycke, J. Sun, and R. Sandstrom, *Nature*, **431**, 672 (2004).
50. E. Vavilova, I. Hellmann, V. Kataev, C. Täschner, B. Büchner, and R. Klingeler, *Phys. Rev., B*, **73**, 144417 (2006).
51. A. I. Popa, E. Vavilova, C. Täschner, V. Kataev, B. Büchner, and R. d. Klingeler, *The Journal of Physical Chemistry C*, **115**, 5265 (2011).
52. S. Demishev, A. Chernobrovkin, V. Glushkov, A. Grigorieva, E. Goodilin, H. Ohta, S. Okubo, M. Fujisawa, T. Sakurai, and N. Sluchanko, *Phys. Rev., B*, **84**, 094426 (2011).
53. L. Lu, X. Han, J. Li, J. Hua, and M. Ouyang, *Journal of Power Sources*, **226**, 272 (2013).
54. P. Viswanathamurthi, N. Bhattarai, H. Y. Kim, and D. R. Lee, *Scripta Materialia*, **49**, 577 (2003).
55. G. Li, S. Pang, L. Jiang, Z. Guo, and Z. Zhang, *J. Phys. Chem. B.*, **110**, 9383 (2006).
56. C. O'Dwyer, D. Navas, V. Lavayen, E. Benavente, M. A. Santa Ana, G. Gonzalez, S. B. Newcomb, and C. M. S. Torres, *Chem. Mater.*, **18**, 3016 (2006).
57. R. Ostermann, D. Li, Y. Yin, J. T. McCann, and Y. Xia, *Nano Letters*, **6**, 1297 (2006).
58. K. Takahashi, S. J. Limmer, Y. Wang, and G. Cao, *J. Phys. Chem. B.*, **108**, 9795 (2004).
59. M. Wakihara, *Materials Science and Engineering: R: Reports*, **33**, 109 (2001).
60. S. Nordlinder, A. Augustsson, T. Schmitt, J. Guo, L. C. Duda, J. Nordgren, T. Gustafsson, and K. Edström, *Chem. Mater.*, **15**, 3227 (2003).
61. M. Malta, G. Louarn, N. Errien, and R. M. Torresi, *Journal of Power Sources*, **156**, 533 (2006).
62. H. J. Muhr, F. Krumeich, U. P. Schönholzer, F. Bieri, M. Niederberger, L. J. Gauckler, and R. Nesper, *Adv. Mater.*, **12**, 231 (2000).
63. M. E. Spahr, P. Stoschitzki-Bitterli, R. Nesper, O. Haas, and P. Novák, *J. Electrochem. Soc.*, **146**, 2780 (1999).
64. S. Nordlinder, L. Nyholm, T. Gustafsson, and K. Edström, *Chem. Mater.*, **18**, 495 (2005).
65. A. Dobley, K. Ngala, S. Yang, P. Y. Zavalij, and M. S. Whittingham, *Chem. Mater.*, **13**, 4382 (2001).
66. P. Simon and Y. Gogotsi, *Nat Mater*, **7**, 845 (2008).
67. A. Liu, M. Ichihara, I. Honma, and H. Zhou, *Electrochem. Commun.*, **9**, 1766 (2007).
68. S. Tepavcevic, H. Xiong, V. R. Stamenkovic, X. Zuo, M. Balasubramanian, V. B. Prakapenka, C. S. Johnson, and T. Rajh, *ACS. Nano.*, **6**, 530 (2011).
69. C. O'Dwyer, V. Lavayen, D. A. Tanner, S. B. Newcomb, E. Benavente, G. Gonzalez, E. Benavente, and C. M. S. Torres, *Adv. Funct. Mater.*, **19**, 1736 (2009).
70. X. Chen, X. Sun, and Y. Li, *Inorganic Chemistry*, **41**, 4524 (2002).
71. G. T. Chandrappa, N. Steunou, S. Cassaignon, C. Bauvais, and J. Livage, *Catal. Today.*, **78**, 85 (2003).
72. D. McNulty, D. N. Buckley, and C. O'Dwyer, *ECS Trans.*, **35**, 237 (2011).
73. M. Wörle, F. Krumeich, F. Bieri, H.-J. Muhr, and R. Nesper, *Zeitschrift fuer anorganische und allgemeine Chemie*, **628**, 2778 (2002).
74. A. Dobley, K. Ngala, S. Yang, P. Y. Zavalij, and M. S. Whittingham, *Chem. Mater.*, **13**, 4382 (2001).

75. L. Mai, W. Chen, Q. Xu, Q. Zhu, C. Han, and J. Peng, *Solid. State. Commun.*, **126**, 541 (2003).
76. V. Petkov, P. Zavalij, S. Lutta, M. Whittingham, V. Parvanov, and S. Shastri, *Phys. Rev., B*, **69**, 085410 (2004).
77. G. Gannon, C. O'Dwyer, J. A. Larsson, and D. Thompson, *J. Phys. Chem. B.*, **115**, 14518 (2011).
78. C. O'Dwyer, G. Gannon, D. McNulty, D. N. Buckley, and D. Thompson, *Chem. Mater.*, **24**, 3981 (2012).
79. D. McNulty, D. N. Buckley, and C. O'Dwyer, *ECS Trans.*, **50**, 165 (2013).
80. M. Armand and J. M. Tarascon, *Nature*, **451**, 652 (2008).
81. X. Liu, C. Huang, J. Qiu, and Y. Wang, *Appl. Surf. Sci.*, **253**, 2747 (2006).
82. W. Chen, J. Peng, L. Mai, Q. Zhu, and Q. Xu, *Mater. Lett.*, **58**, 2275 (2004).
83. C. O'Dwyer, V. Lavayen, M. A. S. Ana, E. Benavente, G. González, and C. M. S. Torres, *J. Electrochem. Soc.*, **154**, K29 (2007).
84. S. Maheshwari, E. Jordan, S. Kumar, F. S. Bates, R. L. Penn, D. F. Shantz, and M. Tsapatsis, *J. Am. Chem. Soc.*, **130**, 1507 (2008).
85. T. Yao, Y. Oka, and N. Yamamoto, *Materials Research Bulletin*, **27**, 669 (1992).
86. W. Chen, L. Q. Mai, J. F. Peng, Q. Xu, and Q. Y. Zhu, *Journal of materials science*, **39**, 2625 (2004).
87. G. Chandrappa, N. Steunou, S. Cassaignon, C. Bauvais, P. K. Biswas, and J. Livage, *Journal of Sol-Gel Science and Technology*, **26**, 593 (2003).
88. A. V. Grigorieva, E. A. Goodilin, A. V. Anikina, I. V. Kolesnik, and Y. D. Tretyakov, *Mendeleev Communications*, **18**, 71 (2008).
89. C. O'Dwyer, V. Lavayen, S. B. Newcomb, M. A. S. Ana, E. Benavente, G. González, and C. M. S. Torres, *Electrochem. Solid-State Lett.*, **10**, A111 (2007).
90. M. S. Whittingham, *J. Electrochem. Soc.*, **123**, 315 (1976).
91. C. Delmas, H. Cognac-Auradou, J. M. Cocciantelli, M. Ménétrier, and J. P. Doumerc, *Solid State Ionics*, **69**, 257 (1994).
92. Y. Wang and G. Cao, *Adv. Mater.*, **20**, 2251 (2008).
93. K. West, B. Zachau-Christiansen, T. Jacobsen, and S. Skaarup, *Electrochim. Acta*, **38**, 1215 (1993).
94. H. X. Li, L. F. Jiao, H. T. Yuan, M. Zhang, J. Guo, L. Q. Wang, M. Zhao, and Y. M. Wang, *Electrochem. Commun.*, **8**, 1693 (2006).
95. J. M. Reinoso, H. J. Muhr, F. Krumeich, F. Bieri, and R. Nesper, *Helvetica Chimica Acta*, **83**, 1724 (2000).
96. S. Nordlinder, K. Edström, and T. Gustafsson, *Electrochem. Solid-State Lett.*, **4**, A129 (2001).
97. Q. Wei, Q. An, D. Chen, L. Mai, S. Chen, Y. Zhao, K. M. Hercule, L. Xu, A. Minhas-Khan, and Q. Zhang, *Nano Lett.*, **14**, 1042 (2014).